Finite Element Simulation of the Motion of a Rigid Body in a Fluid with Free Surface

S. J. Childs

Department of Pure and Applied Mathematics, Rhodes University, Grahamstown, 6140, South Africa

B. D. Reddy

Department of Mathematics and Applied Mathematics, University of Cape Town, Rondebosch, 7700, South Africa

Abstract

In this work a finite element simulation of the motion of a rigid body in a fluid, with free surface, is described. A completely general referential description (of which both Lagrangian and Eulerian descriptions are special cases) of an incompressible, Newtonian fluid is used. Such a description enables a distorting finite element mesh to be used for the deforming fluid domain.

A new scheme for the linearised approximation of the convective term is proposed and the improved, second order accuracy of this scheme is proved. A second theorem, which provides a guideline for the artificial adjustment of the Reynolds number when applying a continuation technique, is also proved. The most effective means of eliminating pressure as a variable and enforcing incompressibility are reviewed. A somewhat novel method to generate finite element meshes automatically about included rigid bodies, and which involves finite element mappings, is described.

The approach taken when approximating the free surface, is that it may be treated as a material entity, that is, the material derivative of the free surface is assumed zero. Euler's equations and conservation of linear momentum are used to determine the motion of the rigid body. A predictor–corrector method is used to solve the combined sub–problems. The resulting model is tested in the context of a driven cavity flow, a driven cavity flow with various, included rigid bodies, a die–swell problem, and a Stokes second order wave.

Keywords: rigid body in a fluid; free surface; incompressible, Newtonian fluid; completely general referential description; arbitrary Lagrangian Eulerian; A.L.E.; finite elements.

1 Introduction

An enormous diversity of problems subscribe to the basic rigid body–fluid–free surface theme (see Figure 1 for a schematic form of the problem of interest). The implications of free surfaces and fluid–rigid body interactions are a deforming fluid domain and the implementation of the majority of numerical time integration schemes then becomes problematic where a purely Eulerian description of the fluid motion has been used. The reason is that most numerical time integration schemes require successive function evaluation at fixed spatial locations. Meshes rapidly snarl when purely Lagrangian descriptions are used.

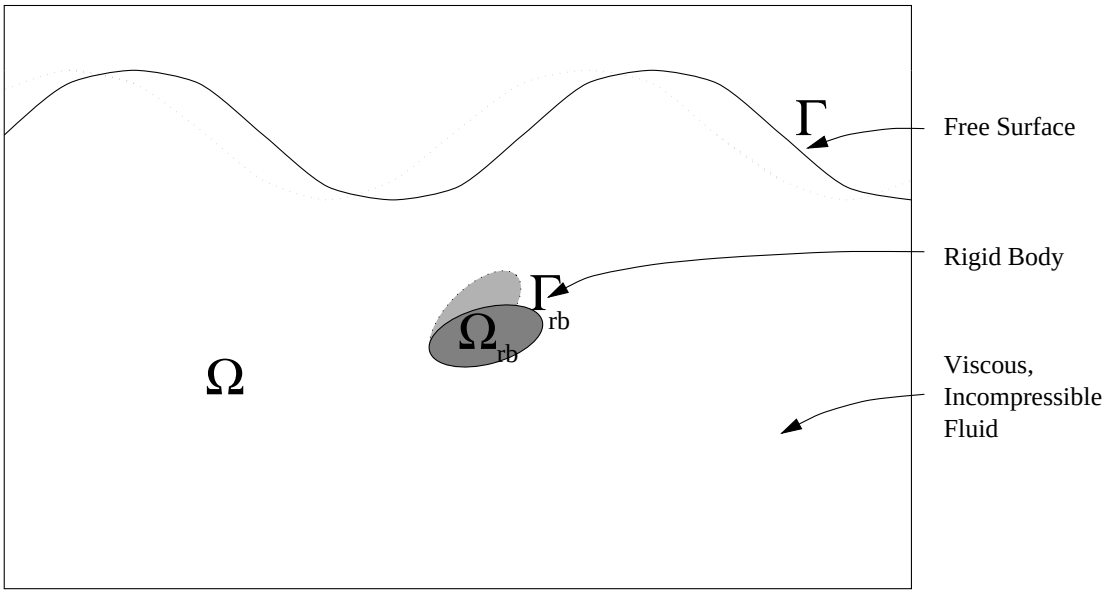

Figure 1: The Motion of a Rigid Body in a Fluid with Free Surface

One alternative is to use the completely general referential description proposed in Childs [3]. Eulerian and Lagrangian references are just two, specific examples of an infinite number of configurations over which to define the fields used to describe the dynamics of deforming continua. They are both special cases of a more general referential description, a description in which a reference configuration is chosen at will (closely related to the so–called arbitrary Lagrangian Eulerian method or A.L.E. method). The completely general referential description is implemented in this work.

Solving for the orientation and position of a rigid body entails solving equations of motion. These are derived from the principles of conservation of angular and linear momentum. Expressing the principle of conservation of angular momentum in more usable terms is not as straight forward as the linear momentum case, and a more appropriate reference must be resorted to. This reference is fixed within the rigid body in such a way that the origin and centre of mass coincide, as do the axes and principal moments of inertia. A complete transformation of all quantities, to this more appropriate reference, is used.

This is in contrast to the approach used in deriving the fluid equations, where quantities are not perceived in terms of the new reference, but instead merely defined to be functions of it. The change of reference is accomplished using a transition matrix and the Coriolis theorem.

The approach taken when approximating the free surface, is that it may be treated as a material entity i.e. the material derivative of the free surface is assumed zero. Surface tension is not considered significant in the free surfaces investigated.

A predictor–corrector method is used to solve the combined rigid body, fluid and free surface sub–problems. A backward difference scheme is used to approximate the time derivative in the fluid sub–problem (in this regard see CHILDS [3]). The finite element method is used for the spatial (referential "space") discretisation. Nonlinearity is circumvented by way of a new second order accurate linearisation, and the use of Picard iteration if necessary. Picard iteration amounts to "linearising" the non–linear term with the solution obtained during the previous iterate. A penalty method is used to eliminate pressure as a variable and a Q_2–P_1 element pair is used as a basis. A somewhat novel method to generate finite element meshes automatically about included rigid bodies, and which involves finite element mappings, is described.

The more conventional methods for solving initial value problems are used to solve for the position and orientation of the rigid body. The definitions of linear and angular velocity are coupled to the equations of motion to produce a system of twelve equations (which are of course also coupled to the fluid equations) and a Runge–Kutta–Fehlberg method is then used. A backward difference scheme and the finite element method are used for the respective temporal and spatial discretisations in the free surface sub–problem.

The overall model was tested in the context of a driven cavity flow, a driven cavity flow with various, included rigid bodies, a die–swell problem and a Stokes, second–order wave. Results for these examples are presented in Section 9. The programme was written by the author in Fortran and originally run on a model 400 Dec Alpha 3100.

2 The Equations Governing the Motion of the Rigid Body

What follows is a brief exposition of the equations of motion. This is, of course, review of classical work contained in a great variety of references. Its inclusion is deemed appropriate not for the sake of completeness alone, but because Euler's equations (the equations governing the angular motion) and the equations governing the translation are written in terms of two distinctly different references.

The equations of motion, six in all, are essentially an explicit re–write of the principles of linear and angular momentum. The equations which govern the translation,

$$\frac{d\boldsymbol{v}_{rb}}{dt} = \frac{1}{m}\Sigma\boldsymbol{f},$$

need no introduction, they being a straight forward statement of the principle of conservation of linear momentum. In the above equation $\boldsymbol{v}_{rb}$ denotes the velocity of the rigid body, m denotes the mass, $\Sigma\boldsymbol{f}$ is the sum of the external forces acting on the rigid body and t denotes time. Expressing the angular momentum equations in a more practicable form is not as straight forward and necessitates the change to the reference already mentioned. The conservation principle of angular momentum may be stated as

$$\frac{d\hat{\boldsymbol{q}}}{dt} = \Sigma(\hat{\boldsymbol{r}} \wedge \hat{\boldsymbol{f}})^{\dagger} \tag{1}$$

where $\hat{\boldsymbol{q}}$ is the angular momentum and $\Sigma(\hat{\boldsymbol{r}} \wedge \hat{\boldsymbol{f}})$ is the sum of the torques which arise as a result of the external forces acting about the centre of mass ($\hat{\boldsymbol{r}}$ is the position vector of a material point within the rigid body and $\hat{\boldsymbol{f}}$ is the force). The equations for the conservation of angular momentum, though easily understood, are not of much use when stated in the above form.

A More Appropriate Reference

The fact that

$$\int_{\Omega_{rb}} \rho\boldsymbol{r}\ d\Omega_{rb} = \boldsymbol{0}$$

for a reference whose origin coincides with the centre of mass (Ω_{rb} is the rigid body domain depicted in Fig. 2) immediately suggests the existence of a more appropriate reference than the one in terms of which the above conservation principle is written. For such a reference fixed within the rigid body,

$$\frac{d\boldsymbol{r}}{dt} = \boldsymbol{0}$$

in addition. This suggests expressing

$$\begin{aligned} \hat{\boldsymbol{q}} &= \int_{\Omega_{rb}} \rho\hat{\boldsymbol{r}} \wedge \hat{\boldsymbol{v}}\ d\hat{\Omega}_{rb} \\ &= \int_{\Omega_{rb}} \rho\hat{\boldsymbol{r}} \wedge \frac{d\hat{\mathbf{r}}}{dt}\ d\hat{\Omega}_{rb} + \int_{\Omega_{rb}} \rho\hat{\boldsymbol{r}}\ d\hat{\Omega}_{rb} \wedge \frac{d\hat{\boldsymbol{x}}}{dt} \end{aligned}$$

in terms of a more appropriate reference. Converting to this new, more appropriate reference by means of the Coriolis theorem, the relation

$$\boldsymbol{q} = \int_{\Omega_{rb}} \rho\boldsymbol{r} \wedge (\boldsymbol{\omega} \wedge \boldsymbol{r}) d\Omega_{rb} \qquad \left(\frac{d\boldsymbol{r}}{dt} = \boldsymbol{0} \quad \textit{for the new reference}\right)$$

is obtained, where $\boldsymbol{\omega}$ is the angular velocity. It is then a fairly elementary exercise to show that

$$\boldsymbol{q} = \boldsymbol{J}\boldsymbol{\omega}, \tag{2}$$

[†]The ˆs are resorted to temporarily in anticipation of the change to the new reference.

where $\boldsymbol{J}$ is the inertia matrix defined by

$$J_{ij} = \int_{\Omega_{rb}} \rho(r_k r_k \delta_{ij} - r_i r_j) d\Omega_{rb}.$$

This result is demonstrated in WOODHOUSE [16].

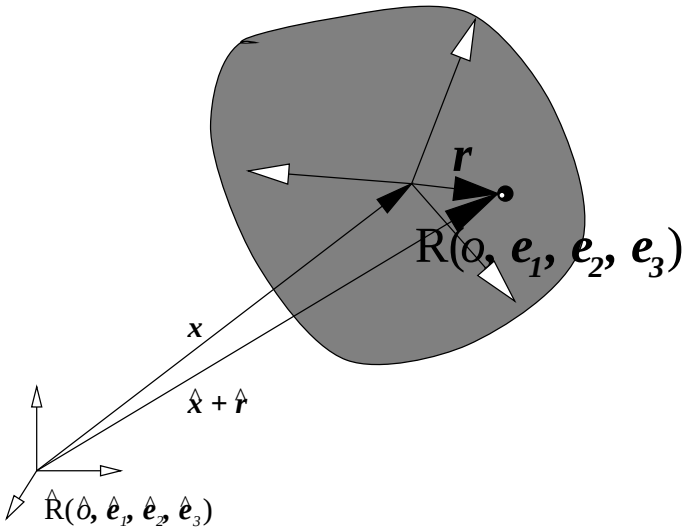

Figure 2: Schematic diagram depicting the position vectors $\boldsymbol{x}$ and $\boldsymbol{r}$ in terms of a more appropriate reference, $R(o, \boldsymbol{e}_1, \boldsymbol{e}_2, \boldsymbol{e}_3)$, which is embedded in the rigid body in such a way that the origin, o, and centre of mass coincide as do the basis vectors and the principal moments of inertia.

Exploring this idea of a more appropriate reference further and restricting it to one, final choice allows still greater simplification; by specifying the basis vectors to coincide with the eigenvectors of the inertia matrix $\boldsymbol{J}(R)$ (i.e. the basis vectors are principal axes), equation (2) reduces to

$$\boldsymbol{q} \;=\; \begin{bmatrix} J_{11}\omega_1 \\ J_{22}\omega_2 \\ J_{33}\omega_3 \end{bmatrix}. \tag{3}$$

Conservation of Angular Momentum in Terms of this More Appropriate Reference

Rewriting equation (1) in terms of this new reference leads firstly to

$$\frac{d\boldsymbol{q}}{dt} + \boldsymbol{\omega} \wedge \boldsymbol{q} \;=\; \Sigma(\boldsymbol{r} \wedge \boldsymbol{f}) \qquad \textit{(by the Coriolis theorem),}$$

which in terms of the relation (3), is

$$\begin{aligned} J_{11}\frac{d\omega_1}{dt} + (J_{33} - J_{22})\omega_2\omega_3 &= \Sigma(\boldsymbol{r} \wedge \boldsymbol{f}) \cdot \boldsymbol{e}_1 \\ J_{22}\frac{d\omega_2}{dt} + (J_{11} - J_{33})\omega_3\omega_1 &= \Sigma(\boldsymbol{r} \wedge \boldsymbol{f}) \cdot \boldsymbol{e}_2 \\ J_{33}\frac{d\omega_3}{dt} + (J_{22} - J_{11})\omega_1\omega_2 &= \Sigma(\boldsymbol{r} \wedge \boldsymbol{f}) \cdot \boldsymbol{e}_3 \end{aligned}$$

where the $J_{ii\ \text{(no contraction)}}$ are the principal moments of inertia defined by

$$\int_{\Omega_{rb}} \rho r_i^2 d\Omega_{rb}.$$

This description is in terms of a reference embedded within the rigid body in such a way that the origin and centre of mass coincide, as do the axes and principal moments of inertia. Failure to recognise this can lead to an incorrect formulation of the forces acting on the rigid body.

3 A Free Surface Description Ignoring Surface Tension

It is assumed that the vertical position of the free surface can be written as a function of horizontal coordinates and time, that is, $x_3 = h(x_1, x_2, t)$. The free surface can be described equivalently by the condition

$$\eta(\boldsymbol{x}, t) \equiv h(x_1, x_2, t) - x_3 = 0.$$

Requiring that the material derivative of this free surface to be zero amounts to writing

$$\frac{\partial h}{\partial t} + \nabla h \cdot [v_1, v_2] = v_3. \tag{4}$$

A physical interpretation of this mathematics is that the free surface is an infinitesimally thin, perfectly elastic skin by which the fluid is contained. The free surface is in actuality not a distinct material entity. The approach is consequently slightly limited. For example, no convection of the free surface is allowed. Restricting the movement of surface nodes to vertical translations alone circumvents having to rewrite the above equations in terms of a completely general referential description.

The variational equations are obtained in the usual manner. Multiplying by an arbitrary function w and integrating, the equations

$$\int_\Gamma w\frac{\partial h}{\partial t}d\Gamma \ + \ \int_\Gamma w\nabla h \cdot [v_1, v_2]d\Gamma \ = \ \int_\Gamma w v_3 d\Gamma$$

are obtained.

Equation (4) is hyperbolic and one would therefore anticipate discontinuities or shocks in the solution. A standard Galerkin type formulation is not sufficient (see Hughes [6], Hughes, Mallet and Mizukami [7] and Johnson [8]) under such circumstances.

The Streamline–Upwind–Petrov–Galerkin (S.U.P.G.) Method with discontinuity capturing is one popular method resorted to when solving hyperbolic equations. This amounts to using

$$w = w^* \ + \ \tau_1(\nabla w^* \cdot \boldsymbol{v}) \ + \ \tau_2(\nabla w^* \cdot \boldsymbol{v}_{tangent}), \qquad \boldsymbol{v}_{tangent} = \frac{\boldsymbol{v} \cdot \nabla h}{|| \nabla h ||^2} \nabla h,$$

where w^* is the arbitrary function in the formulation, τ_1 and τ_2 are constants described in Hughes, Mallet and Mizukami [7].

Hermite elements are one more way in which to obtain smoother surfaces. Hermite elements are used for C^1 approximations which require non–zero first order derivatives at the nodes.

Remark: Although surface tension is not considered significant in the free surfaces to be described in this work, the free surface equations to be used under such circumstances would be

$$(\boldsymbol{\sigma}_1 - \boldsymbol{\sigma}_2) \cdot \frac{\nabla \eta}{|| \nabla \eta ||} = 2G\zeta \frac{\nabla \eta}{|| \nabla \eta ||} + \nabla \zeta$$

where the left hand side is the total traction (the difference between that acting from within and that acting from without) acting on the interface, the last term is a tangential force contribution in instances where surface tension is non-constant, G contains the mean curvature

$$\frac{\partial}{\partial x_1} \left\{ \frac{(\nabla \eta)_1 + (\nabla \eta)_2}{|| \nabla \eta ||} \right\} + \frac{\partial}{\partial x_2} \left\{ \frac{(\nabla \eta)_1 + (\nabla \eta)_2}{|| \nabla \eta ||} \right\},$$

and ζ is the surface tension. See Landau and Lifshitz [12], Bird, Armstrong and Hassager [1] and Joseph and Renardy [9] in this regard.

4 A Completely General Referential Description of an Incompressible, Newtonian Fluid

The implications of free surfaces and fluid–rigid body interactions are a deforming fluid domain and the implementation of the majority of numerical time integration schemes then becomes problematic where a purely Eulerian description of the fluid motion has been used. The reason is that most numerical time integration schemes require successive function evaluation at fixed spatial locations. Meshes rapidly snarl when purely Lagrangian descriptions are used. One alternative is to use a completely general referential description.

The transformation to the completely general reference only involves coordinates where used as spatial variables and the resultant description is therefore inertial in the same way as Lagrangian descriptions are. The conservation principles of mass and linear momentum remain the basis of the fluid model despite having resorted to a completely general reference (as opposed to a conventional Eulerian reference) for the description of the fluid. For the purposes of reading the equations which folow some slightly specialised notation will be introduced.

Notation

In the equations that follow the $\tilde{}$s merely indicate that quantities are functions of a deforming reference, $\tilde{\boldsymbol{x}}$. The operators $\tilde{\nabla}$ and $\widetilde{\text{div}}$ are the referential counterparts of ∇ and div, that is to say that

$$\tilde{\nabla} = \frac{\partial}{\partial \tilde{\boldsymbol{x}}} \qquad \text{and} \qquad \widetilde{\text{div}} = \frac{\partial}{\partial \tilde{x}_1} + \frac{\partial}{\partial \tilde{x}_2} + \frac{\partial}{\partial \tilde{x}_3}.$$

The symbol $\tilde{J}$ is used to denote the determinant of the deformation gradient

$$\tilde{\mathbf{F}} = \frac{\partial \boldsymbol{x}}{\partial \tilde{\boldsymbol{x}}}$$

and the notation $\boldsymbol{A} : \boldsymbol{B}$ is used to denote the matrix inner product $A_{ij}B_{ij}$.

In terms of this newly established notation the conservation principles of linear momentum and mass may be written in primitive form as

$$\rho \left[\frac{\partial \tilde{\boldsymbol{v}}}{\partial t} + \tilde{\nabla}\tilde{\boldsymbol{v}}\tilde{\boldsymbol{F}}^{-1}(\tilde{\boldsymbol{v}} - \tilde{\boldsymbol{v}}^{ref}) \right] \tilde{J} \;=\; \rho \tilde{\boldsymbol{b}} \tilde{J} + \widetilde{\text{div}}\, \tilde{\boldsymbol{P}}$$

and

$$\tilde{\nabla}\tilde{\boldsymbol{v}} : \tilde{\boldsymbol{F}}^{-t} \;=\; 0,$$

where $\tilde{\boldsymbol{P}}$ is the Piola–Kirchoff stress tensor of the first kind, $\tilde{\boldsymbol{P}} = \tilde{\boldsymbol{\sigma}}\tilde{\boldsymbol{F}}^{-t}\tilde{J}$. In terms of the constitutive relation for a Newtonian fluid, $\boldsymbol{\sigma} = -p\boldsymbol{I} + 2\mu\boldsymbol{D}$. Thus

$$\tilde{\boldsymbol{P}} = \left(-p\boldsymbol{I} + \mu \left[\tilde{\nabla}\tilde{\boldsymbol{v}}\tilde{\boldsymbol{F}}^{-1} + \left(\tilde{\nabla}\tilde{\boldsymbol{v}}\tilde{\boldsymbol{F}}^{-1} \right)^t \right] \right) \tilde{\boldsymbol{F}}^{-t}\tilde{J} \qquad \text{since} \qquad \tilde{\boldsymbol{D}} = \frac{1}{2}\left[\widetilde{\nabla \boldsymbol{v}} + \left(\widetilde{\nabla \boldsymbol{v}} \right)^t \right].$$

A comprehensive derivation of these equations is given in Childs [3]. The derivation of a variational formulation is along similar lines to that for the conventional Navier-Stokes equations (the purely Eulerian description).

For a fluid of constant density, the variational formulation

$$\begin{aligned} \rho \int_{\tilde{\Omega}} \tilde{\boldsymbol{w}} \cdot \frac{\partial \tilde{\boldsymbol{v}}}{\partial t} \tilde{J} d\tilde{\Omega} \;+\; \rho \int_{\tilde{\Omega}} \tilde{\boldsymbol{w}} \cdot \tilde{\nabla}\tilde{\boldsymbol{v}} \left[\tilde{\boldsymbol{F}}^{-1}(\tilde{\boldsymbol{v}} - \tilde{\boldsymbol{v}}^{ref}) \right] \tilde{J} d\tilde{\Omega} \;=\; \\ \rho \int_{\tilde{\Omega}} \tilde{\boldsymbol{w}} \cdot \tilde{\boldsymbol{b}} \tilde{J} d\tilde{\Omega} \;+\; \int_{\tilde{\Omega}} \tilde{p} \tilde{\nabla}\tilde{\boldsymbol{w}} : \tilde{\boldsymbol{F}}^{-t} \tilde{J} d\tilde{\Omega} \;-\; 2\mu \int_{\tilde{\Omega}} \tilde{\boldsymbol{D}}(\tilde{\boldsymbol{w}}) : \tilde{\mathbf{D}}(\tilde{\boldsymbol{v}}) \tilde{J} d\tilde{\Omega} \\ + \rho \int_{\tilde{\Gamma}} \tilde{\boldsymbol{w}} \tilde{\boldsymbol{P}} \tilde{\boldsymbol{N}} d\Gamma \end{aligned}$$

$$\int_{\tilde{\Omega}} \tilde{q} \tilde{\nabla}\tilde{\boldsymbol{v}} : \tilde{\boldsymbol{F}}^{-t} d\tilde{\Omega} \;=\; 0$$

is obtained, where $\tilde{q}$ and $\tilde{\boldsymbol{w}}$ are respectively the arbitrary pressure and velocity of the variational formulation. Under the circumstances of a Dirichlet boundary condition the term involving the boundary integral may naturally be omitted.

5 Statement of the Total Problem in Dimensionless Form

Suppose that length is to be measured in units of X and velocity in units of V (which is really parameterising time by $T = \frac{X}{V}$). Then

$$\boldsymbol{x} = \bar{\boldsymbol{x}}X, \qquad \boldsymbol{v} = \bar{\boldsymbol{v}}V \qquad \textit{and} \qquad t = \bar{t}\frac{X}{V}.$$

The equations governing the translation of the rigid body are accordingly divided through by $\frac{V^2}{X}$, the equations governing the rotation by $\rho_s X^3 V^2$, and the fluid equations by $\frac{V^2\rho}{X}$.

Using the symbol $\bar{J}_{ii(\text{no sum})}$ to denote the ith, dimensionless principal moment of inertia of the rigid body,

$$\bar{J}_{ii(\text{no sum})} = \frac{J_{ii(\text{no sum})}}{\rho_s X^5},$$

$\boldsymbol{H}$ to denote the transition matrix for a transition to a reference whose axes coincide with these principal moments of inertia, $\bar{\boldsymbol{c}}$ to denote the centre of mass of the rigid body, $\bar{\Gamma}_{rb}$ to denote the dimensionless surface of the rigid body, $\bar{t}$ to denote a dimensionless time, ρ_f and ρ_s to denote the density of fluid and solid respectively, $\bar{h}$ to denote the dimensionless elevation of a free surface ($\bar{h}$ being a function of a reference prohibited from deforming in a lateral direction i.e. nodes belonging to the free surface move in the vertical only), $\bar{\boldsymbol{v}}$ to denote the dimensionless velocity of the underlying fluid, $\bar{\boldsymbol{F}}$ to denote the deformation gradient, $\bar{J}$ its determinant, $\bar{\boldsymbol{v}}^{mesh}$ to denote the dimensionless velocity of a mesh which is otherwise allowed to deform freely and Re to denote the Reynolds number,

$$Re = \frac{XV\rho_f}{\mu},$$

the combined, dimensionless, free surface–fluid–rigid body problem can then be stated as follows: find $\bar{\boldsymbol{x}}_{rb}$, $\bar{\boldsymbol{\theta}}$, $\bar{\boldsymbol{v}}_{rb}$, $\bar{\boldsymbol{\omega}}$, $\bar{h}$ and $\bar{\boldsymbol{v}}$ (the dimensionless respective position, orientation, velocity and angular velocity of the rigid body, the elevation of the free surface and the

velocity field of the fluid), which satisfy

$$\left.\begin{aligned}
\bar{J}_{11}\frac{d\bar{\omega}_1}{d\bar{t}} \;+\; (\bar{J}_{33} \;-\; \bar{J}_{22})\bar{\omega}_2\bar{\omega}_3 &= \\
&\frac{\rho_f}{\rho_s}\left[\boldsymbol{H}\int_{\bar{\Gamma}_{rb}}(\bar{\boldsymbol{x}}-\bar{\boldsymbol{c}})\wedge\left\{-\bar{p}\boldsymbol{I}+\frac{2}{Re}\bar{\boldsymbol{D}}\right\}\boldsymbol{n}\;d\bar{\Gamma}_{rb}\right]\cdot\boldsymbol{e}_1 \\
\bar{J}_{22}\frac{d\bar{\omega}_2}{d\bar{t}} \;+\; (\bar{J}_{11} \;-\; \bar{J}_{33})\bar{\omega}_3\bar{\omega}_1 &= \\
&\frac{\rho_f}{\rho_s}\left[\boldsymbol{H}\int_{\bar{\Gamma}_{rb}}(\bar{\boldsymbol{x}}-\bar{\boldsymbol{c}})\wedge\left\{-\bar{p}\boldsymbol{I}+\frac{2}{Re}\bar{\boldsymbol{D}}\right\}\boldsymbol{n}\;d\bar{\Gamma}_{rb}\right]\cdot\boldsymbol{e}_2 \\
\bar{J}_{33}\frac{d\bar{\omega}_3}{d\bar{t}} \;+\; (\bar{J}_{22} \;-\; \bar{J}_{11})\bar{\omega}_1\bar{\omega}_2 &= \\
&\frac{\rho_f}{\rho_s}\left[\boldsymbol{H}\int_{\bar{\Gamma}_{rb}}(\bar{\boldsymbol{x}}-\bar{\boldsymbol{c}})\wedge\left\{-\bar{p}\boldsymbol{I}+\frac{2}{Re}\bar{\boldsymbol{D}}\right\}\boldsymbol{n}\;d\bar{\Gamma}_{rb}\right]\cdot\boldsymbol{e}_3 \\
\frac{d\bar{\boldsymbol{v}}_{rb}}{d\bar{t}} &= \frac{\rho_f}{\bar{m}\rho_s}\int_{\bar{\Gamma}_{rb}}\left\{-\bar{p}\boldsymbol{I}+\frac{2}{Re}\bar{\boldsymbol{D}}\right\}\boldsymbol{n}\;d\bar{\Gamma}_{rb}+\frac{X}{V^2}\boldsymbol{b} \\
\frac{d\bar{\boldsymbol{\theta}}}{dt} &= \bar{\boldsymbol{\omega}} \\
\frac{d\bar{\boldsymbol{x}}_{rb}}{dt} &= \bar{\boldsymbol{v}}_{rb}
\end{aligned}\right\}\quad\text{Included Rigid Body}$$

$$\left.\frac{\partial\bar{h}}{\partial\bar{t}}+\bar{\nabla}\bar{h}\cdot[\bar{v}_1,\bar{v}_2]=\bar{v}_3\right\}\quad\text{Free Surface}$$

$$\left.\begin{aligned}
\left[\frac{\partial\bar{\boldsymbol{v}}}{\partial\bar{t}}+\bar{\nabla}\bar{\boldsymbol{v}}\bar{\boldsymbol{F}}^{-1}(\bar{\boldsymbol{v}}-\bar{\boldsymbol{v}}^{mesh})\right]\bar{J} &= \frac{X}{V^2}\boldsymbol{b}\bar{J}+\bar{\mathrm{div}}\,\bar{\boldsymbol{P}} \\
\bar{\nabla}\bar{\boldsymbol{v}}:\bar{\boldsymbol{F}}^{-t} &= 0
\end{aligned}\right\}\quad\text{Fluid}$$

where

$$\left.\bar{\boldsymbol{P}} \;=\; \bar{\boldsymbol{\sigma}}\bar{\boldsymbol{F}}^{-t}\bar{J} \;=\; \left(-\bar{p}\boldsymbol{I}+\frac{2}{Re}\left[\bar{\nabla}\bar{\boldsymbol{v}}\bar{\boldsymbol{F}}^{-1}+\left(\bar{\nabla}\bar{\boldsymbol{v}}\bar{\boldsymbol{F}}^{-1}\right)^t\right]\right)\bar{\boldsymbol{F}}^{-t}\bar{J}\right\}\quad\text{Fluid}$$

subject to the "no slip" requirements

$$\bar{\boldsymbol{v}}\mid_{\bar{\Gamma}_{rb}} \;=\; \bar{\boldsymbol{v}}_{rb}+\bar{\boldsymbol{\omega}}\wedge(\bar{\boldsymbol{x}}-\bar{\boldsymbol{c}})$$

at fluid–rigid body interfaces and

$$\bar{\boldsymbol{v}}\mid_{\bar{\Gamma}} \;=\; \boldsymbol{0}$$

at fixed, solid impermeable boundaries. Additional boundary conditions depend on the problem in question.

6 Approximate Fluid Equation and its Implementation

Two topics which are relevant to the approximate fluid equation are dealing with the nonlinearity of the convective term and enforcing incompressibility in such a way as to eliminate pressure as a variable. Only against such a background can the approximate fluid equation be written.

6.1 The Incompressibility Condition

Two methods to enforce incompressibility and eliminate pressure as a variable are considered relevant for review. The use of either a penalty method or an iterative, augmented Lagrangian method both have distinct, yet different advantages.

The L.B.B. or B.B. condition (so named after Ladyzhenskaya, Babuška and Brezzi) must be taken into account in the implementation of either method. So–called "locking" or "chequerboard" modes can arise in the event of the L.B.B. condition not being satisfied. Work by authors such as Oden, Kikuchi and Song [13] can be referred to for a more in-depth treatment of the L.B.B. condition.

A penalty method was used to eliminate pressure as a variable and enforce incompressibility in later examples, despite the acclaimed superiority of the iterative augmented Lagrangian approach (discussed shortly). The results obtained using the more efficient and more easily implemented penalty method compared favourably with those obtained by Simo and Armero [15], who used the iterative augmented Lagrangian approach. In other examples the penalty method was used for reasons of standardisation (so that results could be compared against those cited in the literature).

The Simple Penalty Method

Penalty methods are closely related to the artificial compressibility method and provide a remarkably simple strategy for solving the equations. A fundamental assumption made in using the penalty method is that the incompressibility condition,

$$\operatorname{div} \boldsymbol{v} = 0,$$

can be replaced by one of small incompressibility,

$$\operatorname{div} \boldsymbol{v} = -\epsilon p,$$

where ϵ is small. (It is tempting to substitute this expression for p in the momentum equations immediately, thereby eliminating the pressure from the equations altogether

at an analytic stage and prior to construction. This would circumvent the complicated construction which otherwise results. If such an approach were to be taken, however, the L.B.B. condition would not be satisfied and an appropriate underintegration rule would then be necessary to avoid an approximation which will lead to "locking" or "chequer board" modes.)

The corresponding variational, small incompressibility is

$$\int_\Omega q \operatorname{div} \boldsymbol{v} d\Omega = -\epsilon \int_\Omega qp d\Omega$$

where q is the arbitrary function of the variational formulation. A well known shortcoming of penalty methods is the severe ill–conditioning which occurs as the penalty parameter is decreased, making the simulation of exact incompressibility practically impossible. As the theoretical limit $\epsilon = 0$, an infinite condition number for the discrete algebraic system is obtained. Despite this shortcoming a straight forward penalty method provides a remarkably easy–to–implement means of enforcing incompressibility and eliminating pressure as a variable, furthermore, there was no discernable difference between results obtained using the penalty method and those obtained using the iterative augmented Lagrangian approach for the driven cavity flow problem (compare the results in Subsection 9.1 with those obtained by Simo and Armero [15]).

An Iterative Augmented Lagrangian Approach for Enforcing Exact Incompressibility

There is considerable merit in the iterative augmented Lagrangian approach from the point of view of realising theory. Incompressibility can be exactly enforced (to within a specified tolerance) for finite values of the penalty parameter using an iterative augmented Lagrangian approach. This is in contrast to conventional penalty formulations where there is a trade–off between enforcing exact incompressibility and obtaining a severely ill–conditioned algebraic system.

A fundamental assumption made in using the iterative augmented Lagrangian method is that the incompressibility condition can be replaced by one of iterative, limiting–case incompressibility,

$$\operatorname{div} \boldsymbol{v} = -\epsilon \left(p^{(k+1)} - p^{(k)} \right)$$

for ϵ small.

The method of augmented Lagrangians provides an effective means to circumvent the shortcomings of the simple penalty method and enables the divergence free constraint to be exactly enforced for finite values of the penalty parameter.

6.2 A New, Linear Scheme for the Approximation of the Convective Term

The following theorem is the first of two proposed numerical improvements (originally presented in Childs and Reddy [4]). Linearising with a guess obtained by extrapolating

through solutions from the previous two time steps leads to second order accuracy. This is an improvement on the conventional method by an order of magnitude.

THEOREM 1 *The linearised terms,* $(2\boldsymbol{v}\mid_t - \boldsymbol{v}\mid_{t-\Delta t})\cdot\nabla\boldsymbol{v}\mid_{t+\Delta t}$ *and* $\boldsymbol{v}\mid_{t+\Delta t}\cdot\nabla(2\boldsymbol{v}\mid_t - \boldsymbol{v}\mid_{t-\Delta t})$*, are second order accurate (have error* $O(\Delta t^2)$*) approximations of the nonlinear term* $(\boldsymbol{v}\cdot\nabla\boldsymbol{v})\mid_{t+\Delta t}$*.*

PROOF:

$$\begin{aligned}
\boldsymbol{v}\mid_{t+\Delta t} &= \boldsymbol{v}\mid_t + \Delta t \left.\frac{\partial \boldsymbol{v}}{\partial t}\right|_t + O(\Delta t^2) && \textit{(by Taylor series)} \\
&= \boldsymbol{v}\mid_t + \Delta t \left(\frac{\boldsymbol{v}\mid_t - \boldsymbol{v}\mid_{t-\Delta t}}{\Delta t} + O(\Delta t)\right) + O(\Delta t^2) && \textit{(using a backward difference)} \\
&= 2\boldsymbol{v}\mid_t - \boldsymbol{v}\mid_{t-\Delta t} + O(\Delta t^2)
\end{aligned}$$

$$\begin{aligned}
(\boldsymbol{v}\cdot\nabla\boldsymbol{v})\mid_{t+\Delta t} &= \left[2\boldsymbol{v}\mid_t - \boldsymbol{v}\mid_{t-\Delta t} + O(\Delta t^2)\right]\cdot\nabla\boldsymbol{v}\mid_{t+\Delta t} \\
&= [2\boldsymbol{v}\mid_t - \boldsymbol{v}\mid_{t-\Delta t}]\cdot\nabla\boldsymbol{v}\mid_{t+\Delta t} + O(\Delta t^2)
\end{aligned}$$

The above linearisation schemes are an improvement on the conventional $\boldsymbol{v}\mid_t\cdot\nabla\boldsymbol{v}\mid_{t+\Delta t}$ [†] or $\boldsymbol{v}\mid_{t+\Delta t}\cdot\nabla\boldsymbol{v}\mid_t$ linearisation schemes by an order of magnitude.

Further refinement of this second order accurate solution can usually be accomplished by the process of Picard iteration, if necessary – providing the initial guess lies within a radius of convergence. Picard iteration amounts to "linearising" the nonlinear term with the solution obtained during the previous iterate.

6.3 Approximate Fluid Equation

An updated approach and the choice of a referential configuration which coincides with the spatial configuration at the instant within each time step about which the equations are to be evaluated, facilitates the elimination of the deformation gradient from the resulting fluid scheme completely (under such conditions the deformation gradient becomes identity – see CHILDS [3]).

A backward difference is used to approximate the time derivative in accordance with the findings of CHILDS [3]. The finite element method is used for the spatial (referential "space" – the reference deforms) discretisation and a Q_2–P_1 element pair is the chosen basis. A penalty method is used to eliminate pressure as a variable. The approximate

[†]Favoured in terms of both rate and radius of convergence by CUVELIER, SEGAL and VAN STEENHOVEN [5].

equations, to be solved for the nodal velocities, V_j^e (pertaining to element e), are consequently

$$\begin{aligned}\mathop{\mathsf{A}}_{e=1}^{E}\Big\{\frac{1}{\Delta t}\int_{\hat\Omega} B_{ki}B_{kj}J^e d\hat\Omega \;&+\; \int_{\hat\Omega} B_{ki}G_{kjl}B_{lm}J^e d\hat\Omega (V_m^{e\ linearisation}-V_m^{e\ mesh})\\ &+\; \frac{1}{\epsilon}\left[\int_{\hat\Omega}\varphi_m\varphi_l J^e d\hat\Omega\right]^{-1}\int_{\hat\Omega}\varphi_m G_{kjk}J^e d\hat\Omega\int_{\hat\Omega}\varphi_l G_{nin}J^e d\hat\Omega\\ &+\; \frac{2}{Re}\int_{\hat\Omega}\left(G_{kil}+G_{lik}\right)\left(G_{kjl}+G_{ljk}\right)J^e d\hat\Omega\Big\}\mathop{\mathsf{A}}_{e=1}^{E} V_j^e\\ =\ \mathop{\mathsf{A}}_{e=1}^{E}\Big\{\int_{\hat\Omega} g\ B_{ki}B_{k3}J^e d\hat\Omega\ &+\ \frac{1}{\Delta t}\int_{\hat\Omega} B_{ki}B_{kj}J^e d\hat\Omega\left(V_j^e|_{t-\Delta t}\right)\Big\},\end{aligned}$$

where A is the element assembly operator, E is the total number of elements, e, into which the domain has been subdivided, $\hat\Omega$ is the master element domain, Δt is the length of the time step, the $\phi_i(\boldsymbol{\xi})$ are the basis functions, $\{\boldsymbol{\xi}\}$ is the master element coordinate system,

$$\boldsymbol{B}(\boldsymbol{\xi})=\begin{bmatrix}\phi_1 & 0 & 0 & \dots & \phi_n & 0 & 0\\ 0 & \phi_1 & 0 & \dots & 0 & \phi_n & 0\\ 0 & 0 & \phi_1 & \dots & 0 & 0 & \phi_n\end{bmatrix},\qquad \boldsymbol{\varphi}(\boldsymbol{\xi})=[1,x_1(\boldsymbol{\xi}),x_2(\boldsymbol{\xi}),x_3(\boldsymbol{\xi})]^{\dagger},$$

$$G_{ikj}(\boldsymbol{\xi})=\frac{\partial B_{ik}}{\partial\xi_l}\frac{\xi_l}{\partial x_j}=\frac{\partial B_{ik}}{\partial x_j}(\boldsymbol{\xi}),\qquad J^e=\det\left\{\frac{\partial \boldsymbol{x}}{\partial\boldsymbol{\xi}}\right\}\ \text{for element } e,\qquad Re=\frac{XV\rho}{\mu},$$

n is the number of nodes on each element, μ is viscosity, ρ is density, X, V are a length scale and a velocity scale respectively, $\boldsymbol{V}^{e\ linearisation}$ is the new second order accurate linearisation (given in Subsection 6.2),

$$\boldsymbol{V}^{e\ linearisation}=2\boldsymbol{V}^e\ |_t-\boldsymbol{V}^e\ |_{t-\Delta t},$$

$\boldsymbol{V}^{e\ mesh}$ is the mesh velocity, ϵ is the penalty parameter ($\epsilon=10^{-6}$) and g is the gravitational acceleration.

To recover the pressure on each element once the velocity solution has been obtained,

$$p=-\frac{1}{\epsilon}\left[\int_{\hat\Omega}\varphi_m\varphi_l J^e d\hat\Omega\right]^{-1}\int_{\hat\Omega}\varphi_m G_{kjk}J^e d\hat\Omega\ V_j^e\ \varphi_l. \tag{5}$$

6.4 A Guideline for Artificial Reynolds Number Adjustment

A straight forward Picard iteration process (in which the convective term is linearised) may not be sufficient at higher Reynolds numbers where the nonlinear term becomes

[†]The Q_2–P_1 element pair was shown to satisfy the L.B.B. condition in the context of rectangular elements. It is important to note in this regard that a linear function mapped from the master element using a Q_2 mapping will no longer be P_1 for non–rectangular elements.

more significant and the radius of convergence is smaller. What one has to do under such circumstances is implement a continuation technique. That is, lower the Reynolds number to a level where convergence is attainable, then raise it incrementally, obtaining progressively better solutions at each stage. Choosing these various artificial Reynolds number levels can, however, turn out to be somewhat problematic. What follows was devised as a guideline in making this choice. Suppose the nonlinear and linear parts of the equations are expressed in terms of two matrices, $\boldsymbol{A}$ and $\boldsymbol{B}$, respectively. The equations to be solved are then

$$A_{nkj}v_k v_j + B_{nj}v_j + c_n = 0.$$

THEOREM 2 *A sufficient condition for the iterative linearisation method to converge is*

$$|| \boldsymbol{D} ||_p < 1$$

where

$$D_{jl} = (A_{nkj}v_k^{i-1} - B_{nj})^{-1} A_{nlm} v_m^{i-1},$$

$|| \ . \ ||_p$ *denotes the generalised p norm and the superscript i denotes the number of the iteration from which a given solution was obtained (*CHILDS *and* REDDY *[4]).*

PROOF: Let $\boldsymbol{\epsilon}^{i-1}$ denote the difference between the solutions obtained from the ith and $(i-1)$th iterations. That is,

$$\boldsymbol{\epsilon}^{i-1} = \boldsymbol{v}^i - \boldsymbol{v}^{i-1}$$

The system of equations solved at the $(i-1)$th Picard iterate was accordingly

$$\begin{aligned} A_{nkj}v_k^{i-2}v_j^{i-1} + B_{nj}v_j^{i-1} + c_n &= 0 \\ A_{nkj}(v_k^{i-1} - \epsilon_k^{i-2})v_j^{i-1} + B_{nj}v_j^{i-1} + c_n &= 0. \end{aligned} \tag{6}$$

The system of equations to be solved at the ith Picard iterate is

$$\begin{aligned} A_{nkj}v_k^{i-1}v_j^{i} + B_{nj}v_j^{i} + c_n &= 0 \\ A_{nkj}v_k^{i-1}(v_j^{i-1} + \epsilon_j^{i-1}) + B_{nj}(v_j^{i-1} + \epsilon_j^{i-1}) + c_n &= 0. \end{aligned} \tag{7}$$

Equating (6) with (7),

$$\begin{aligned} A_{nkj}v_k^{i-1}\epsilon_j^{i-1} + B_{nj}\epsilon_j^{i-1} &= -A_{nkj}\epsilon_k^{i-2}v_j^{i-1} \\ \epsilon_j^{i-1} &= -(A_{nkj}v_k^{i-1} + B_{nj})^{-1}A_{nlm}\epsilon_l^{i-2}v_m^{i-1} \\ &= D_{jl}\epsilon_l^{i-2} \\ || \boldsymbol{\epsilon}^{i-1} ||_p &\leq || \boldsymbol{D} ||_p \, || \boldsymbol{\epsilon}^{i-2} ||_p \, . \end{aligned}$$

A sufficient requirement for convergence is therefore

$$|| \boldsymbol{\epsilon}^{i-1} ||_p < || \boldsymbol{\epsilon}^{i-2} ||_p \quad \Leftrightarrow \quad || \boldsymbol{D} ||_p < 1$$

COROLLARY 1 *A sufficient condition for the iterative linearisation method to converge is*

$$\max_{l} \ \Sigma_{j=1}^{n} \mid (A_{nkj} v_k^{i-1} - B_{nj})^{-1} A_{nlm} v_m^{i-1} \mid < 1$$

(the maximum absolute column sum < 1), where the superscript i denotes the number of the iteration from which that particular solution was obtained.

PROOF: In the particular instance of the 1 vector norm,

$$|| \ \boldsymbol{D} \ ||_1 = \max_{l} \ \Sigma_{j=1}^{n} \mid (A_{nkj} v_k^{i-1} - B_{nj})^{-1} A_{nlm} v_m^{i-1} \mid$$

(The natural matrix norm induced by the 1 vector norm is the maximum absolute column sum.)

REMARK: This guideline serves only to examine local convergence, and one still has to hunt for a suitable Reynolds number by trial and error. It does, however, is provide an exact quantitative measure of this local convergence and, depending on the solver used, can improve efficiency.

7 A Predictor–Corrector or "Linearised" Approach

The combined free surface–fluid–rigid body problem is highly nonlinear. An important decision had to be taken on whether to solve the respective sub–problems simultaneously, using a Newton–Raphson method, or separately using a predictor–corrector (iterative) approach. The latter approach may be justified in terms of a Picard-type linearisation process (similar to that discussed in Section 6.2 when dealing with the convective term).

The advantages of a predictor–corrector approach over solving simultaneously (the approach taken by many) are expected to be a larger radius of convergence and hence a more robust scheme, substantially less code and easy, separate testing of sub–problems.

The disadvantages of a predictor–corrector approach over solving simultaneously are expected to be linear, as opposed to quadratic, rates of convergence. The expected slow rate of convergence could possibly be overcome to a degree by taking good initial guesses based on previous solutions, using linear extrapolation for example.

7.1 The Resulting Algorithm

Figure 3 outlines the algorithm which results from the use of such a linearised approach. The solution values of the fluid sub–problem are used in solving the free surface sub–problem, working out the traction on the rigid body and consequently in solving the rigid body sub–problem. The mesh is then adjusted accordingly and, if not the first iteration, the convergence is examined. If only the first iteration, alternatively, if the degree of convergence is found to be unsatisfactory, the process is repeated. Once this iteration process has converged, a new time step is commenced.

The $O(\Delta t^4)$ Runge–Kutta–Fehlberg and Adams–Moulton approximations used in the rigid body sub–problem are possibly excessive in comparison to the $O(\Delta t)$ finite difference schemes implemented in the fluid and free surface problems.

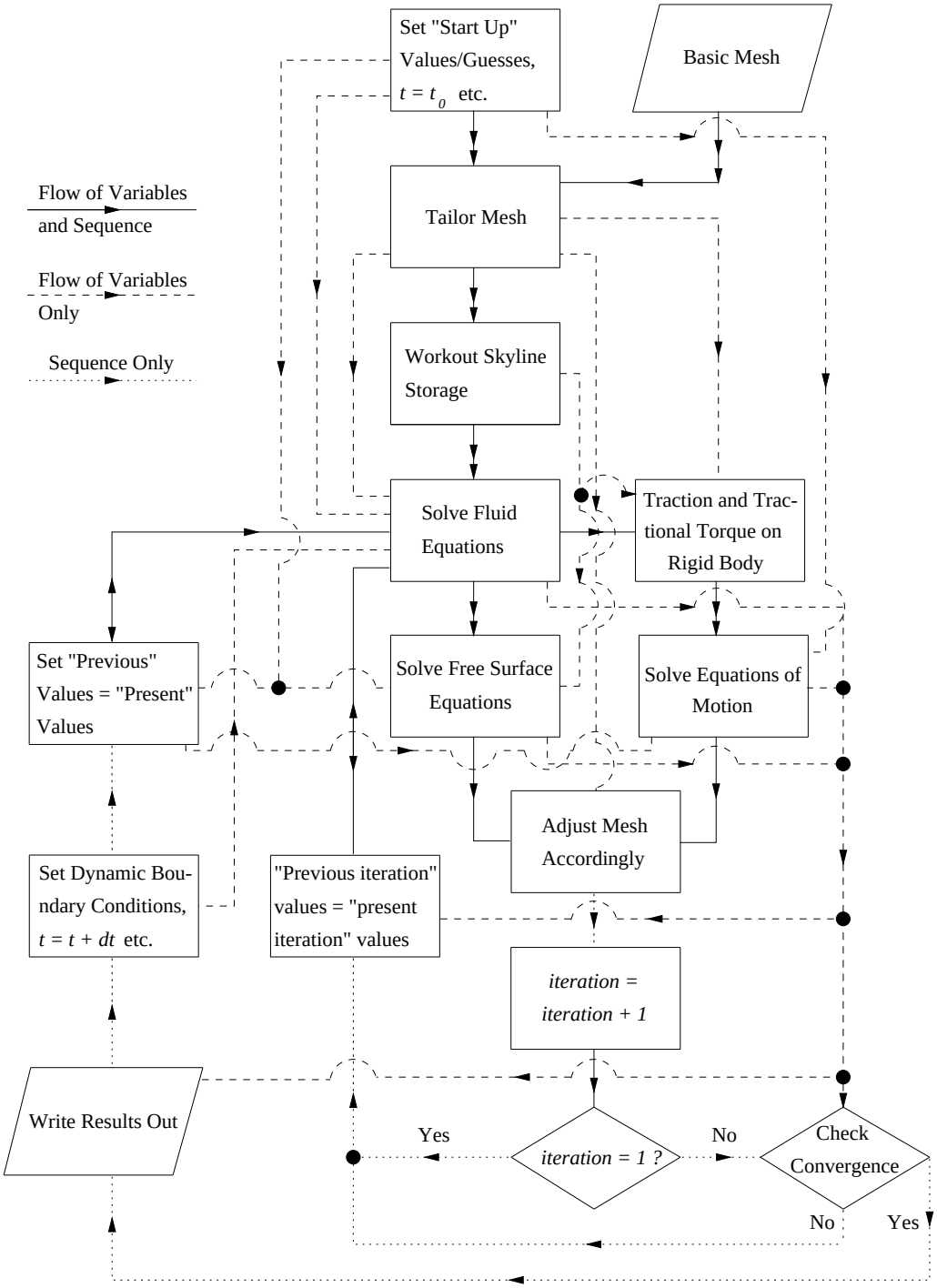

Figure 3: Combined Structure–Flow Chart Outlining the Predictor–Corrector Algorithm for the Fluid–Rigid–Body–Free Surface Problem.

8 Automatic Mesh Generation About Included Bodies of Any Shape

The finite element mesh was automatically generated and adjusted about the included rigid body in what is possibly a slightly novel fashion. A small region of mesh immediately adjacent to the included rigid body was repeatedly remapped to cope with the changing orientation, the remainder was squashed/stretched according to the translation.

Local Distortion About an Included Rigid Body

The local distortion about included rigid bodies is obtained by mapping four square chunks of rectangular mesh to the four wedge–shaped domains depicted in Figure 4 using finite element mappings. A square region of mesh centered on, and including the rigid body, is first removed. Each of the depicted wedge–shaped regions is then demarcated by as many points as there are nodes in an element i.e. each wedge shaped–region is set up as a massive element.

Demarcation: Demarcation is accomplished by first locating the intersection of the lines which bisect corners and edges of the square frame, with the surface of the rigid body using Newton's method. The remainder of this demarcation process needs no explanation.

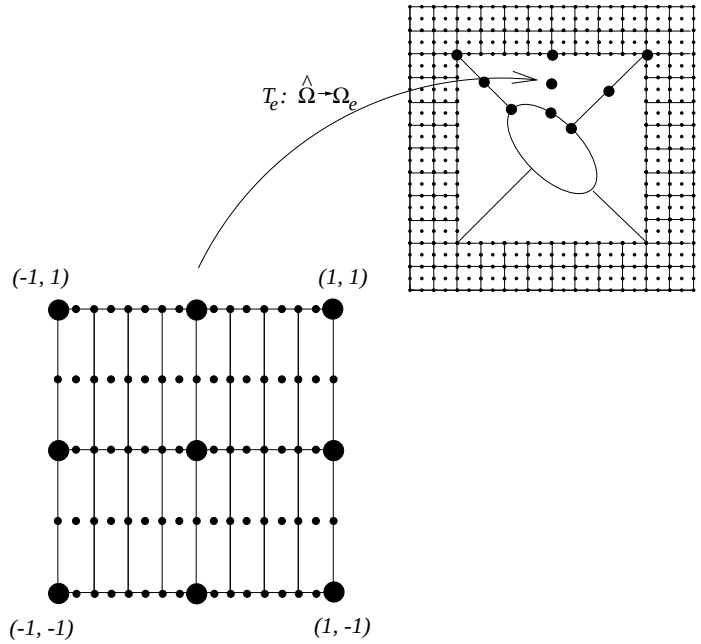

Figure 4: The Local Distortion is Obtained by Mapping Square Chunks of Rectangular Mesh Using Finite Element Mappings.

Mapping: Chunks of uniform mesh, which have identical extremities to those of the master element, are then mapped into the newly–demarcated, wedge–shaped regions using finite element mappings. The devised method maps chunks of uniform mesh into wedge–shaped regions surrounding the included rigid body in exactly the same manner as points in the master element domain are, in theory, mapped into individual mesh elements. In the finite element mapping,

$$\begin{aligned} T_e : \hat{\Omega} &\rightarrow \Omega_e \\ \boldsymbol{x}(\boldsymbol{\xi}) &= \sum_{i=1}^{nNode} \boldsymbol{x}_i \phi_i(\boldsymbol{\xi}), \end{aligned}$$

symbols which previously denoted the master element, the master element variables, the corresponding position in the domain, the position of node i and element e now denote the following: $\hat{\Omega}$ – the chunk of uniform mesh, $\boldsymbol{\xi}$ – the position of a constituent node in the chunk, $\boldsymbol{x}$ – the corresponding position in the wedge, $\boldsymbol{x}_i$ – the position of the ith point demarcating the wedge and Ω_e – the wedge.

Interface Adjustment: Further fine adjustment of nodes intended to delineate the surface of the rigid body is accomplished by moving them along a line between node and centre, to the rigid body surface using Newton's method, thereby accomodating additional shape complexity.

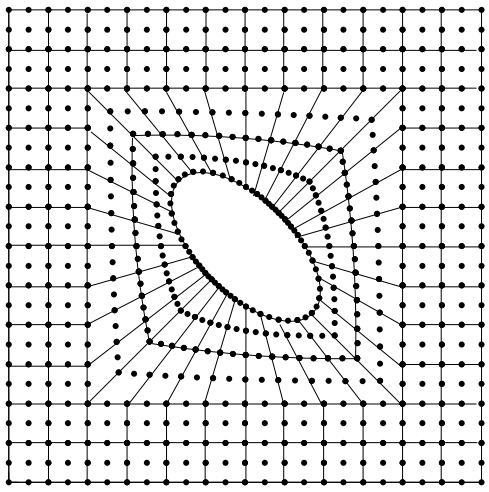

Figure 5: Automatic Mesh Generation about a Rigid Body which is Simultaneously Rotating and Translating.

The method described was found to be remarkably practical, simple and effective with maximum angles never exceeding $\frac{\pi}{4}$ radians at element vertices within the mesh.

Translational Mesh Deformation

The mesh outside the "box" (the box containing the 4 "wedges" enclosing the rigid body) is squashed/stretched according to the requirements of the translation (the nodes are translated in the same direction by a factor inversely proportional to their distance from the box).

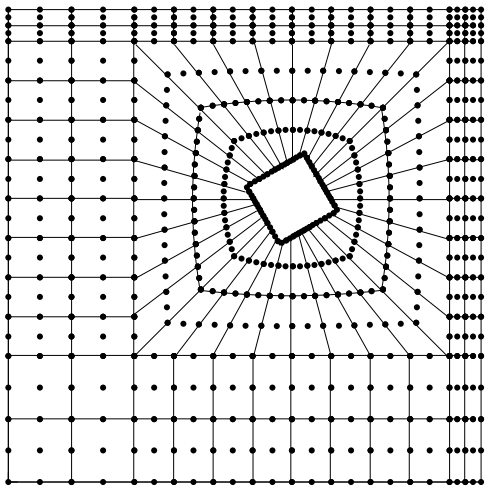

Figure 6: Automatic Mesh Generation and Adjustment about a Diamond which is Simultaneously Rotating and Translating.

9 Some Test Examples

The final model was tested in the context of a driven cavity flow, a driven cavity flow with various, included rigid bodies, a die–swell problem and a Stokes, second–order wave. The idea was to use as simple as possible flows at extremely low Reynolds numbers, so as to generate the smoothest possible flows in which any resulting rigid body motion could be expected to be highly predictable, alternatively examples for which there exist well established results.

9.1 Example 1: Driven Cavity Flow

A variety of bench-mark tests for viscous, incompressible flows are cited in the literature. The driven cavity flows of Carey and Krishnan [2] and Simo and Armero [15] are two

such examples. The so–called "leaky lid" driven cavity flow of SIMO ET. AL. was found to be the more sensitive of the two when testing the performance of schemes approximating the Navier–Stokes equations. In addition, SIMO ET. AL. tested the scheme for the Navier-Stokes equations rigorously using the leaky lid problem.

These results could be used as a comparison in testing the performance of the completely general referential description derived in CHILDS [3] as well as to compare the performance of the standard, penalty method (used here) with that of the iterative, augmented Lagrangian approach (used by SIMO ET. AL.). The main objective of these tests was nonetheless to generate and study as smooth as possible a flow into which a somewhat inconsequential (flow–wise inconsequential) rigid body could later be introduced (see the forthcoming example).

REMARK: Both the above mentioned flows are steady in the context of the traditional Eulerian description. They are, however, "unsteady" in the context of a deforming mesh, a factor enhancing their potential as tests.

The problem is that of a square, two–dimensional "pot" whose lid is moved across the top at a rate equal to its diameter for a Reynolds number of unity. The boundary conditions are accordingly "no slip" on container walls and a horizontal flow of unity across the top (as depicted in Figure 7). The problem also bears a certain resemblance to an idealised pothole in a river bed. A mesh consisting of one hundred and forty four elements was deformed at differing rates (also depicted in Figure 7).

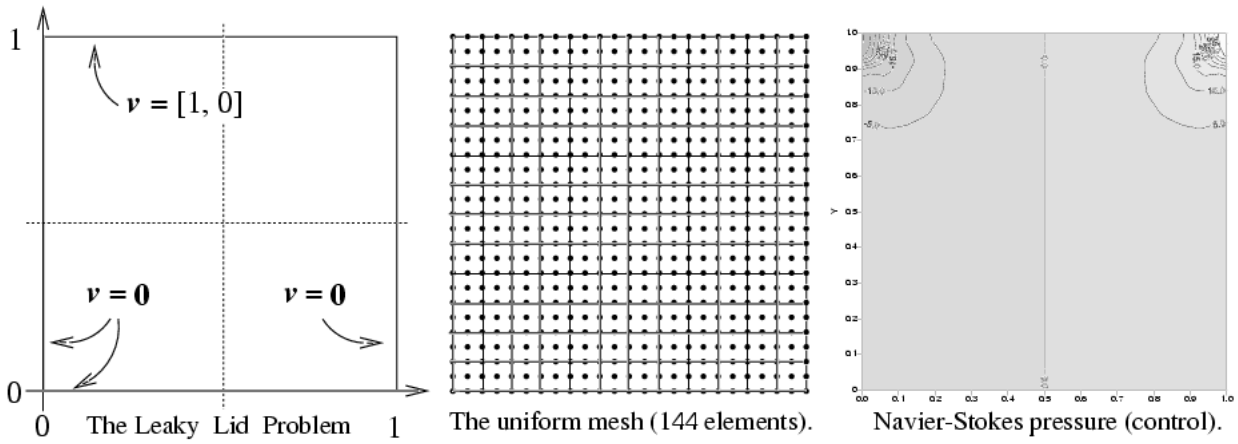

Figure 7: The Problem, the Mesh and the Pressures Obtained Using the Conventional Eulerian Equations.

Results

The results in Figures 8, 9 and 10 obtained while deforming the 144 element mesh depicted, are in agreement with those obtained using the analogous Navier–Stokes algorithm on a fixed uniform mesh (the control results in Figure 7 and the relevant velocity profiles

in Figure 10 on page 23). They are also in agreement with the results of Simo and Armero [15], obtained using the Navier–Stokes equations (the conventional Eulerian description) on a fixed, uniform mesh consisting of 3200 triangular elements.

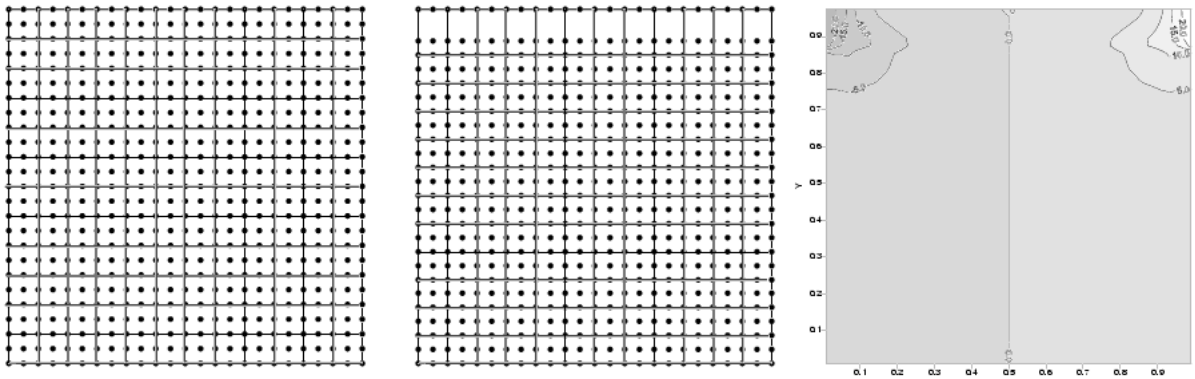

The uniform mesh (144 elements) at the start of the test time step.

The distorted mesh (144 elements) at the end of the test time step.

Pressure for a 5% mesh compression.

Figure 8: Pressures Obtained Using the Completely General Referential Equation.

The fixed, uniform mesh, with which the control results were obtained, consisted of 144 9–noded, quadrilateral elements. In the first test all, but the 25 upper boundary nodes, were compressed into the lower 95 % of the problem domain after which the mesh was restored to a uniform state.

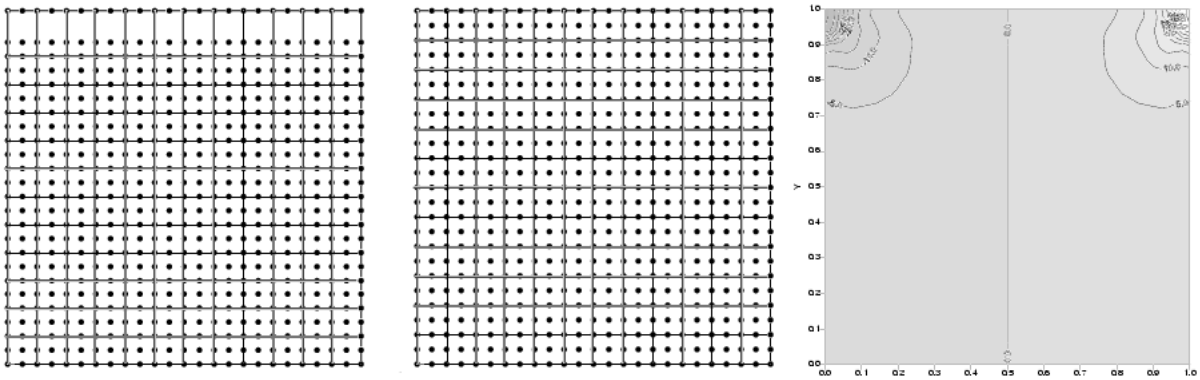

The distorted mesh (144 elements) at the start of the next time step.

The uniform mesh (144 elements) at the end of the next time step.

Pressure for a 5% mesh decompression.

Figure 9: Pressures Obtained Using the Completely General Referential Equation.

The mesh was successively compressed and decompressed over two time steps, each of length 0.05. Mesh velocities were therefore of the order of 10 times greater than the flow velocities being modelled.

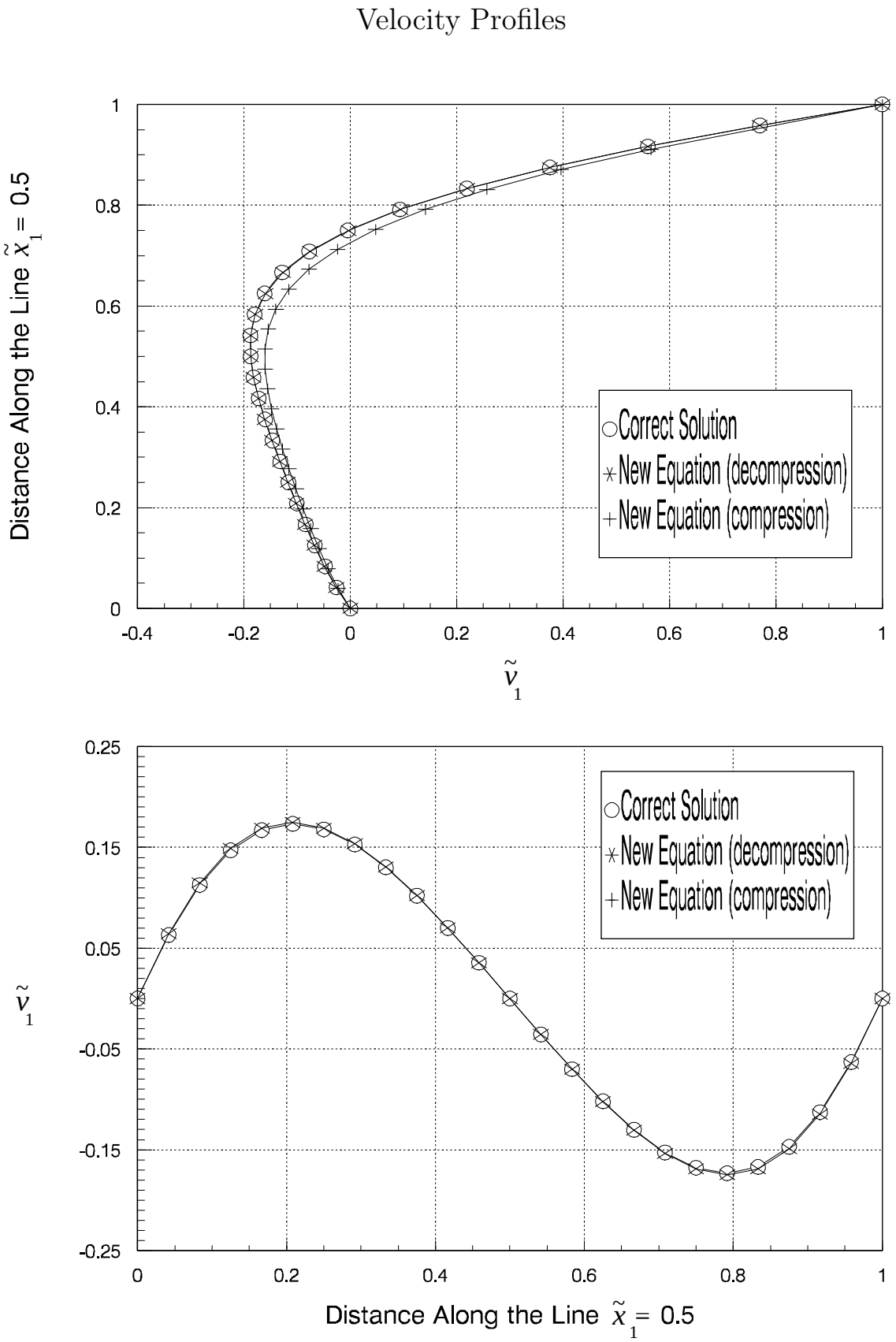

Figure 10: In this test part of the mesh was successively compressed and decompressed by 5 % over two time steps of length 0.05.

In the second test (Figs. 11, 12 and 13) all but 25 boundary nodes were compressed into the lower three quarters of the domain after which the mesh was restored to a uniform state.

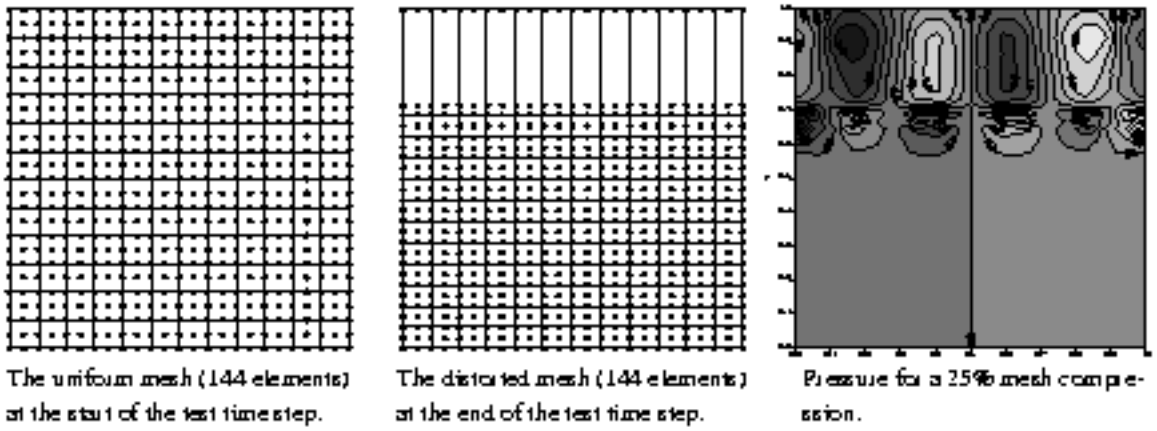

Figure 11: Pressures Obtained Using the Completely General Referential Equation.

In this example the mesh was successively compressed and decompressed by 25 % over two time steps of length 0.05. Mesh velocities were therefore of the order of 50 times greater than the flow velocities being modelled.

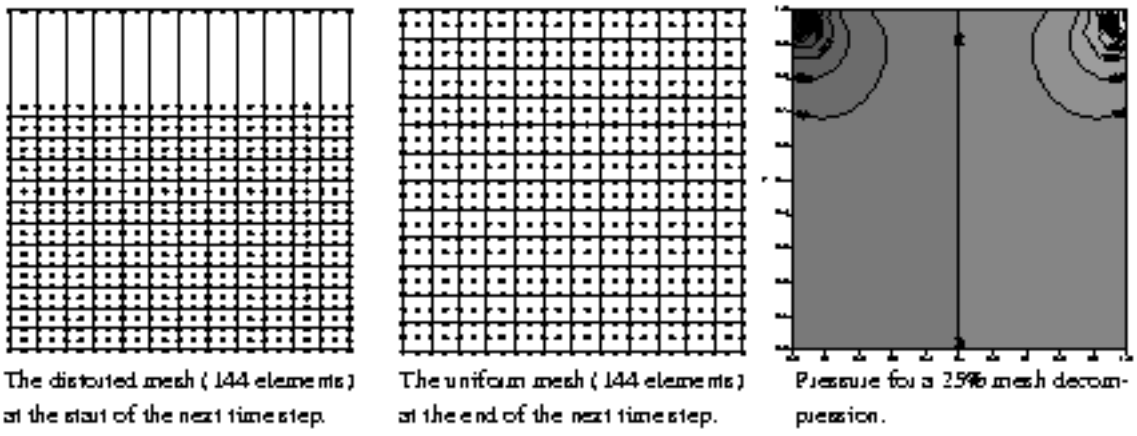

Figure 12: Pressures Obtained Using the Completely General Referential Equation.

The error is attributed to a combination of a bad mesh (mostly) and relatively high off–scale mesh velocities. It should be remembered that a bad mesh is a bad mesh nonetheless.

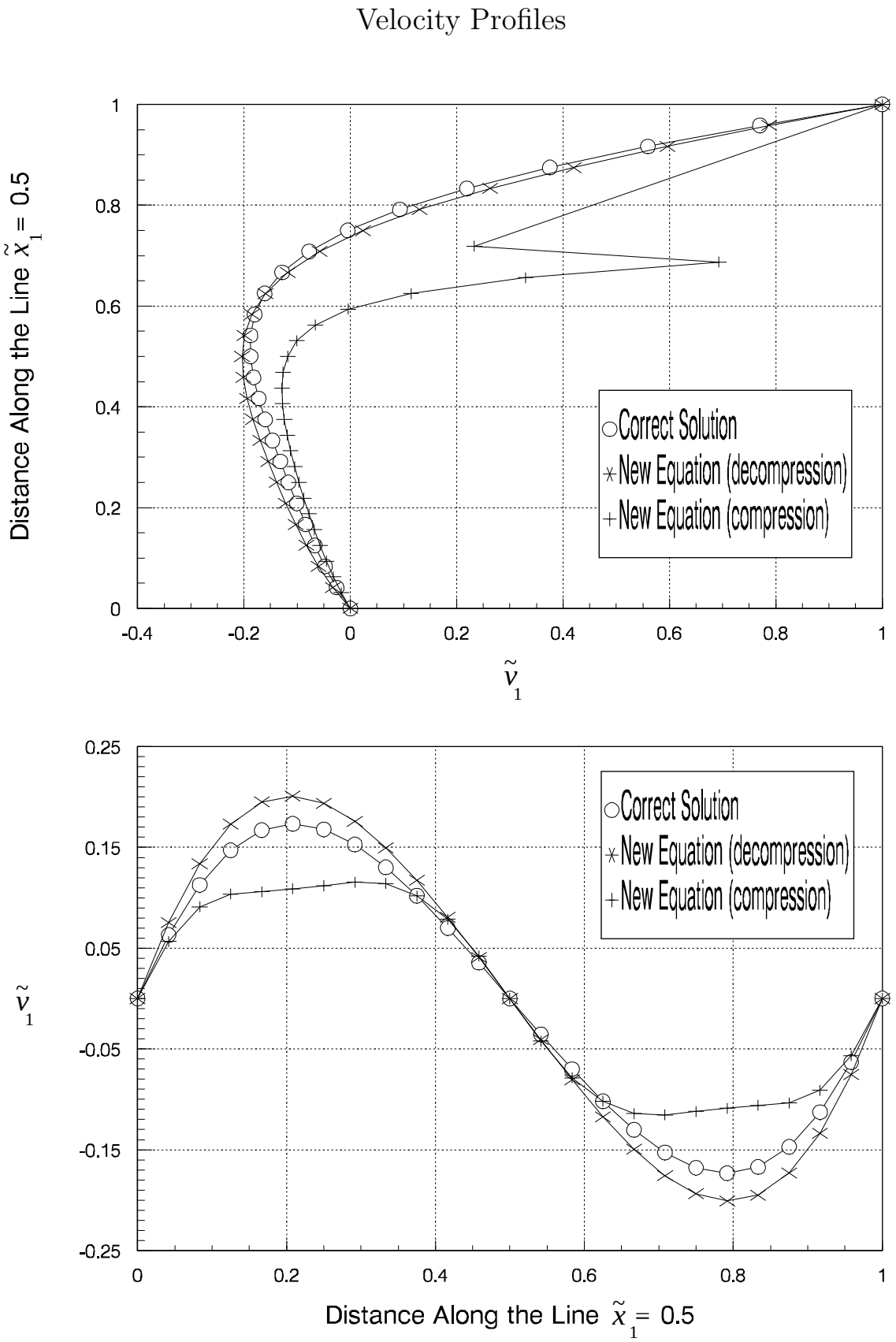

Figure 13: In this test part of the mesh was successively compressed and decompressed by 25 % over two time steps of length 0.05.

REMARK: A further fact illustrated by the results of this test is that, of the pressure and velocity solutions, the pressure solution is the more sensitive of the two. This is to be expected since the pressure is recovered from what is fundamentally a difference in something like the tenth decimal place of the velocity solution (see equation (5)) depending on the penalty parameter.

9.2 Example 2: "Pebble in a Pothole"

In this example rigid bodies of varying mass and moments of inertia were released from rest in a flow dictated by the same boundary conditions as the driven cavity flow of the previous example. One would expect a "die bead" (a small rigid body of neutral bouyancy) to move in tandem with the fluid soon after its release from rest. One might also expect a clockwise spinning to be induced by concentrating the mass closer to the centre i.e. lowering the moment of inertia.

Various rigid bodies were introduced to the cavity driven flow problem described in Subsection 9.1, in the absence of a body force. Although the algorithm allows for the inclusion of a rigid body of any shape, one which could be expected to behave fairly predictably was selected for the purposes of the test. The results presented shortly involve the elliptical rod–shaped body

$$\frac{x_1^2}{2^2} + \frac{x_2^2}{1^2} = 0.025^2,$$

whose major axis is 0.1.

Results

The results which follow were in agreement with the notion that the die bead would move in tandem with the fluid soon after its release from rest. In the succesive trajectories in Figure 14 the mass was successively concentrated closer to the centre (a lower moment of inertia was used). A clockwise spin was then induced.

The last trajectory in Figure 14 was obtained using a Reynolds number of unity in order to generate a smooth, predictable flow as close as possible to the driven cavity flow of Subsection 14. Although the scaling is not immediately reminiscent of any real life problem, the example serves to further verify the potential of the methods described qualitatively.

The results for the included rigid body tests were extremely encouraging. This is especially so when it is considered that the Reynolds numbers implied by small, included rigid bodies are low and the model being developed is eventually intended to elucidate problems of a sedimentological nature.

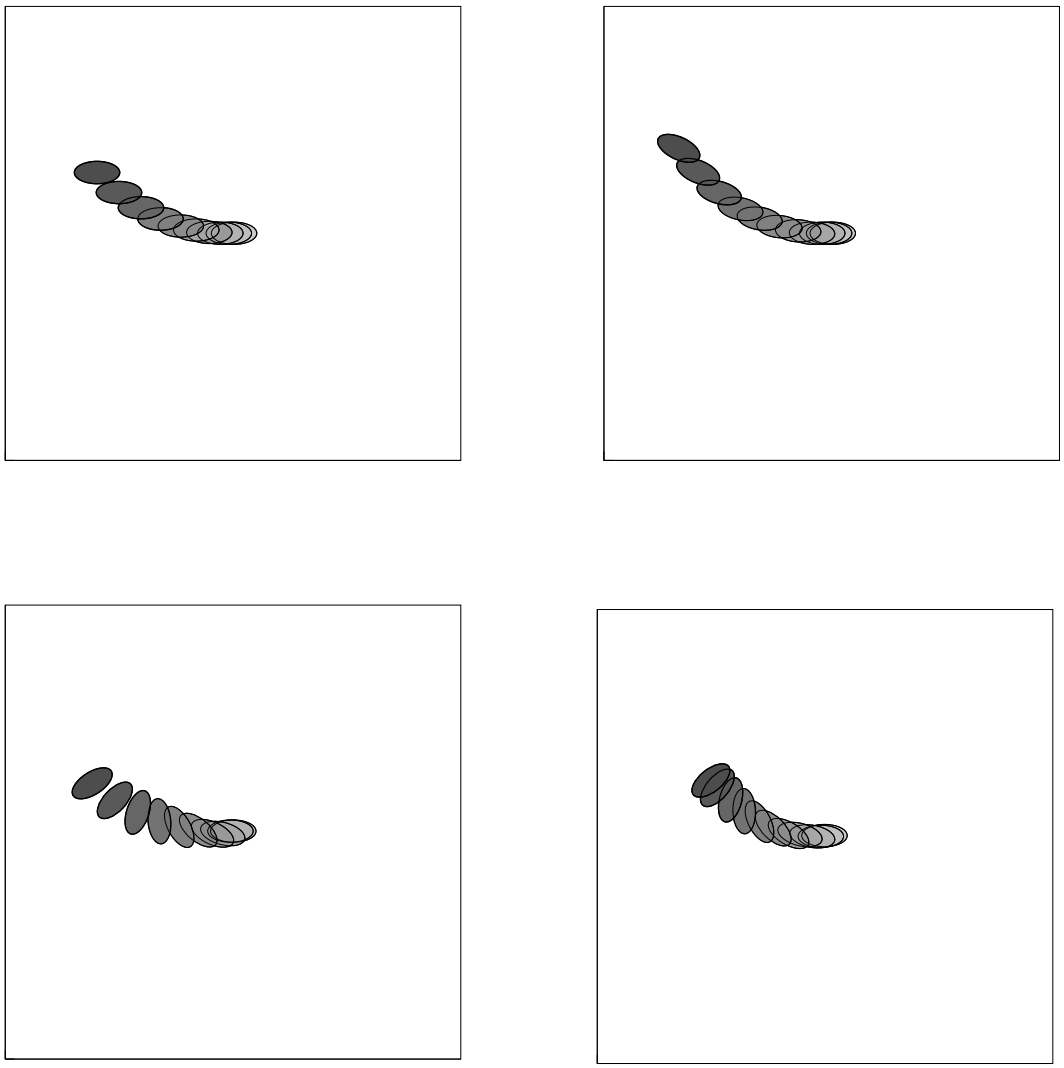

Figure 14: The trajectories of various included rigid bodies released from rest at the centre of the driven cavity flow described in Subsection 9.1. TOP LEFT: $Re = 0.025$, $\bar{m} = 251.3$, $\bar{J}_{33} = 314.2$ and $t = 3.6$ secs. TOP RIGHT: $Re = 0.025$, $\bar{m} = 251.3$, $\bar{J}_{33} = 1.0$ and $t = 4.0$ secs. BOTTOM LEFT: $Re = 0.025$, $\bar{m} = 251.3$, $\bar{J}_{33} = 0.1$ and $t = 3.6$ secs. BOTTOM RIGHT: $Re = 1$, $\bar{m} = 1$, moment of inertia (scaled) $= 0.1$ and $t = 2.0$ secs.

9.3 Example 3: Die Swell Problems

The axis–symmetric die swell (or fluid jet) problem is a free surface problem well documented in the literature. The exact details of the problem description always differ to varying degrees, however, the central theme basic to all involves the extrusion of a fluid with initial parabolic flow profile from the end of a short nozzle. The various boundaries in terms of which this particular version is specified are depicted in Figure 15.

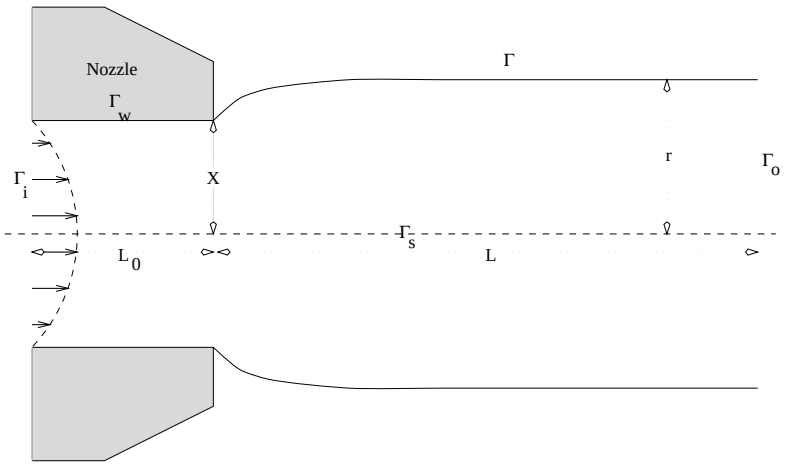

Figure 15: The Die Swell Problem

At the free surface, Γ:

$$h\,|_{x_1=0} = X$$

$$\left.\frac{dh}{dx_1}\right|_{x_1=L} = 0$$

At the nozzle wall, Γ_w:

$$\boldsymbol{v} = 0$$

At the inlet, Γ_i:

$$v_1 = \frac{3}{2}V\left(1-\frac{x_2^2}{X^2}\right)$$

$$= \frac{3}{2}\frac{\mu}{\rho X}Re\left(1-\frac{x_2^2}{X^2}\right)$$

$$v_2 = 0$$

At the outlet, Γ_o:

$$\boldsymbol{\sigma n}\cdot\boldsymbol{n} = 0 \qquad (=\ \bar{\boldsymbol{P}}\bar{\boldsymbol{N}}\cdot\bar{\boldsymbol{N}})$$

$$\boldsymbol{v}\cdot\boldsymbol{t} = 0 \qquad (=\ \bar{\boldsymbol{v}}\cdot\bar{\boldsymbol{T}})$$

At the symmetry axis, Γ_s:

$$\boldsymbol{\sigma n}\cdot\boldsymbol{t} = 0 \qquad (=\ \bar{\boldsymbol{P}}\bar{\boldsymbol{N}}\cdot\bar{\boldsymbol{T}})$$

$$\boldsymbol{v}\cdot\boldsymbol{n} = 0 \qquad (=\ \bar{\boldsymbol{v}}\cdot\bar{\boldsymbol{N}})$$

The Symmetry Axis, Γ_s: Simultaneous implementation of both Γ_s boundary conditions amounts to leaving the term

$$\int_{\bar{\Gamma}_s} \bar{\boldsymbol{w}} \cdot \bar{\boldsymbol{P}}\bar{\boldsymbol{N}} \; d\bar{\Gamma}_s$$

out of the fluid equations and specifying $\bar{\boldsymbol{v}} \cdot \bar{\boldsymbol{N}}$, the component of velocity normal to the boundary. Because the boundary condition is Dirichlet in the normal direction, variational formulation is consequently not required in that direction. This allows $\bar{\boldsymbol{w}}$ in

$$\int_{\bar{\Gamma}_s} \bar{\boldsymbol{w}} \cdot \bar{\boldsymbol{P}}\bar{\boldsymbol{N}} \; d\bar{\Gamma}_s = \int_{\bar{\Gamma}_s} (\bar{\boldsymbol{P}}\bar{\boldsymbol{N}} \cdot \bar{\boldsymbol{N}})(\bar{\boldsymbol{w}} \cdot \bar{\boldsymbol{N}}) \; d\bar{\Gamma}_s + \int_{\bar{\Gamma}_s} (\bar{\boldsymbol{P}}\bar{\boldsymbol{N}} \cdot \bar{\boldsymbol{T}})(\bar{\boldsymbol{w}} \cdot \bar{\boldsymbol{T}}) \; d\bar{\Gamma}_s \tag{8}$$

to be chosen arbitrarily, but in such a way that $\bar{\boldsymbol{w}} \cdot \bar{\boldsymbol{N}} = 0$.

The Outlet, Γ_o: Implementing both Γ_o boundary conditions simultaneously amounts to omitting the term

$$\int_{\Gamma_o} \bar{\boldsymbol{w}} \cdot \bar{\boldsymbol{P}}\bar{\boldsymbol{N}} \; d\Gamma_o$$

and specifying $\bar{\boldsymbol{v}} \cdot \bar{\boldsymbol{T}}$. This implementation can be justified in a likewise fashion to that given for the boundary condition at the symmetry axis.

Results

Examples of die swell problems in which $X = 1$, $L_o = 3.5$ and $L = 20$ for various kinematic viscosities and/or velocity scales were examined using a 150 (50×3) element mesh. The predicted die swell ratios agree well with those obtained by other, more specific methods.

Compare [1] the result of Omodei [14], Figure 5 (on page 87) with the corresponding $Re = 1$ result depicted in Figure 16, for example. Good agreement is obtained between Omodei's Figure 7 (on page 88) result and the corresponding $Re = 10$ result depicted in Figure 17, likewise between his Figure 8 (on page 89) result and the corresponding $Re = 18$ result depicted in Figure 18. These results are further substantiated by those of Kruyt, Cuvelier, Segal and Van Der Zanden [11], and those of Engelman and Dupret quoted in Kruyt et al..

[1] Care needs to be taken in matching inlet velocity profiles as well as scales when comparing results.

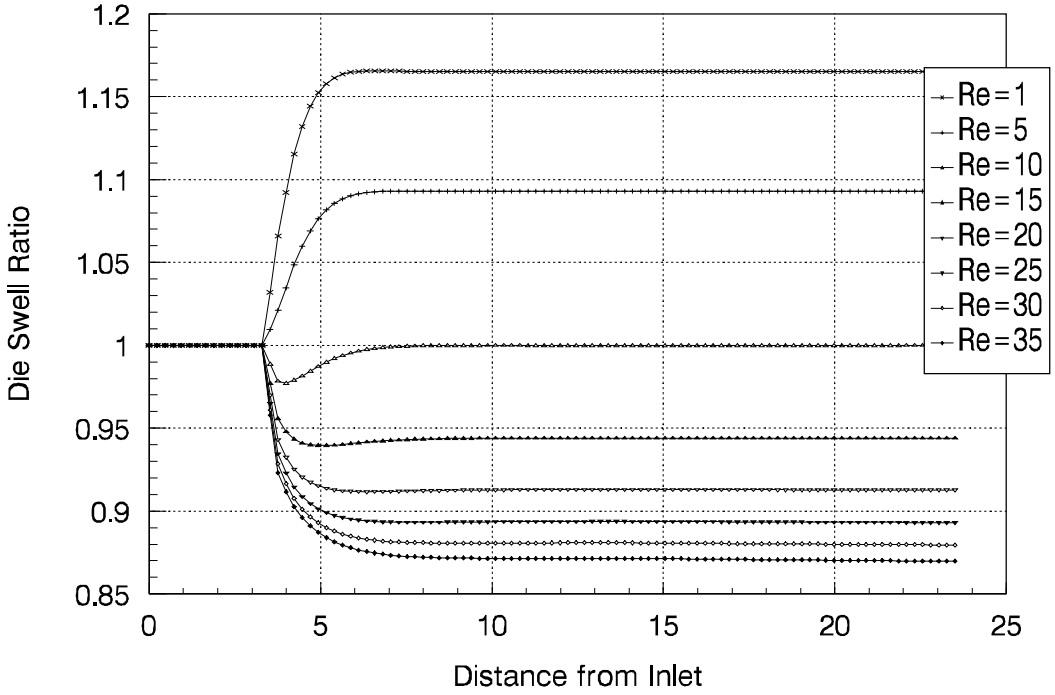

Figure 16: Die swell ratios predicted for various Reynolds numbers using an inlet velocity profile of $\bar{v}_1 = \frac{Re}{1}\frac{3}{2}(1-\bar{x}_2^2)$ and the methods described.

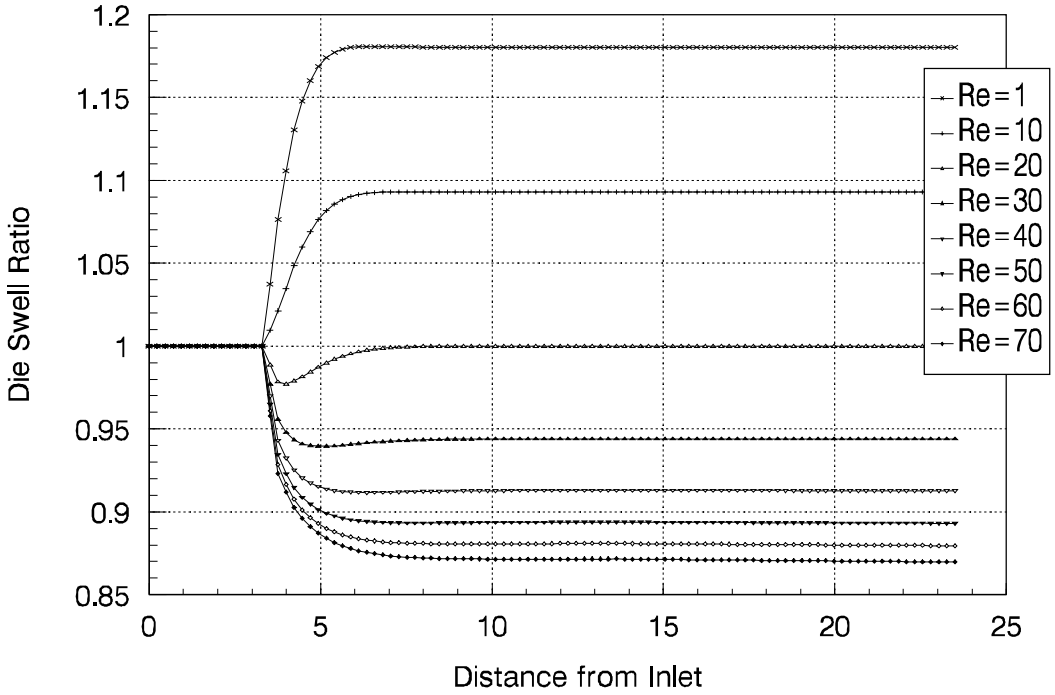

Figure 17: Die swell ratios predicted for various Reynolds numbers using an inlet velocity profile of $\bar{v}_1 = \frac{Re}{10}\frac{3}{2}(1-\bar{x}_2^2)$ and the methods described.

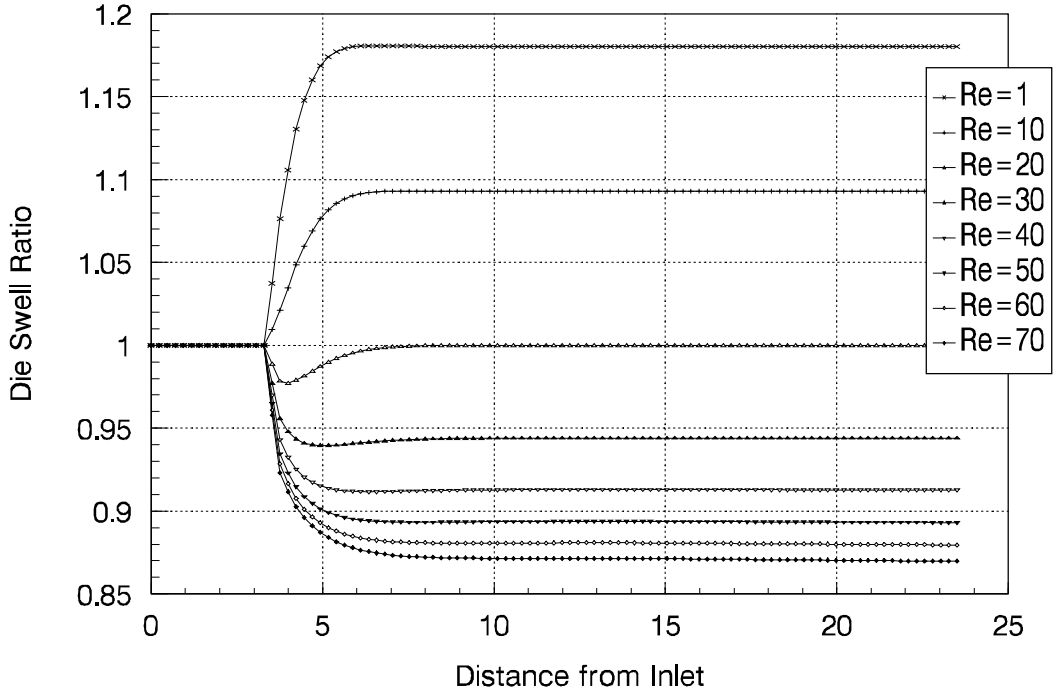

Figure 18: Die swell ratios predicted for various Reynolds numbers using an inlet velocity profile of $\bar{v}_1 = \frac{Re}{20}\frac{3}{2}(1 - \bar{x}_2^2)$ and the methods described.

9.4 Example 4: A Stokes Second Order Wave

In this test the velocity profile and surface elevation predicted by Stokes second order wave theory were used as boundary conditions for flow and free surface subproblems respectively. The development of Stokes second order theory is the same as that of Airy wave (Stokes first order) theory, the exception being that terms as far as second order ($O\left[\frac{H^2}{\lambda^2}\right]$) in the power series expansion of the velocity potential are used. Wave troughs are consequently flatter and the crests are sharper than those predicted using the corresponding first order theory (see KOUTITAS [10] in this regard).

Results

The method converged rapidly to the Stokes second order surface (Figure 19 on page 32) in the initial stages, despite the use of some fairly preposterous free surface starting guesses. This was found to be so for a range of wave lengths, amplitudes and domains experimented with. The problem was, however, not attempted with the same seriousness as previous examples and the mesh was poor (there being only three elements in the vertical extent of the mesh). Problems with wave propagation were consequently experienced as time progressed.

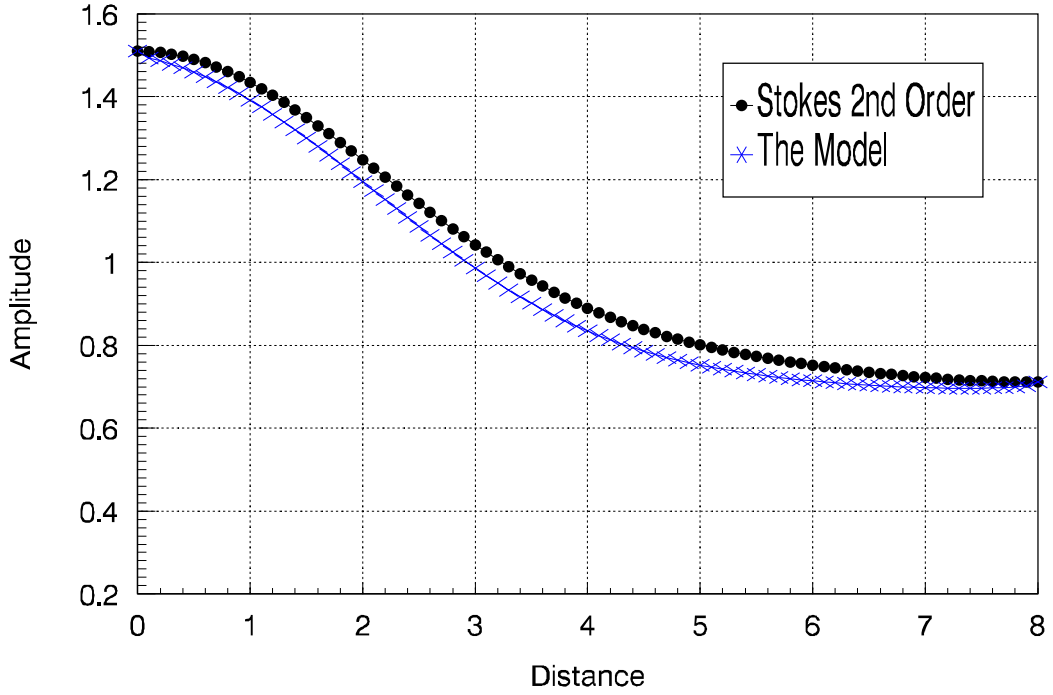

Figure 19: A Stokes Second Order Wave.

10 Conclusions

The completely general referential description proposed in Childs [3] is varified by the numerical experiments of Section 9, as was the predictor–corrector approach proposed in Section 7. Although the resources at the authors disposal limited the tests to two dimensional problems, this is not expected to be of any consequence.

The linearised terms $(2\boldsymbol{v}\mid_t - \boldsymbol{v}\mid_{t-\Delta t})\cdot\nabla\boldsymbol{v}\mid_{t+\Delta t}$ and $\boldsymbol{v}\mid_{t+\Delta t}\cdot\nabla(2\boldsymbol{v}\mid_t - \boldsymbol{v}\mid_{t-\Delta t})$ are second order accurate approximations of the convective term. The formula given in Theorem 2 provides an exact quantitative measure of local convergence for a given Reynolds number when applying a continuation technique and, depending on the solver used, can improve efficiency.

The more efficient and more easily implemented penalty method was found to produce comparable results to the iterative augmented Lagrangian approach (through which incompressibility can be exactly enforced) in the simple test examples performed. With regard to the L.B.B. condition, it is important to note that a linear basis function mapped from the master element using a Q_2 mapping will no longer be P_1 for non–rectangular elements (the Q_2–P_1 element pair was shown to satisfy the L.B.B. condition in the context of rectangular elements).

The holistic method to automatically generate meshes about rigid bodies included within the fluid, using finite element mappings, was found to be remarkably practical, simple and effective with maximum angles within the mesh never exceeding $\frac{\pi}{4}$ radians (outlined

in Section 8).

References

[1] R. B. Bird, R. C. Armstrong, and O. Hassager. Dynamics of polymeric liquids. *Fluid Mechanics, 2nd edn, Wiley, New York*, 1, 1987.

[2] G. F. Carey and R. Krishnan. Penalty approximation of Stokes flow. *Computer Methods in Applied Mechanics and Engineering*, 35:169–206, 1981.

[3] S. J. Childs. The energetic implications of using deforming reference descriptions to simulate the motion of viscous incompressible fluids. *in review, International Journal of Numerical Methods in Fluids*, 1998.

[4] S. J. Childs and B. D. Reddy. Finite element simulation of a rigid body in a fluid with free surface. *Proceedings of the 1st South African Conference on Applied Mechanics '96*, pages 190–197, 1996.

[5] C. Cuvelier, A. Segal, and A. A. van Steenhoven. *Finite Element Methods and Navier–Stokes Equations*. D. Reidel Publishing Company, Dordrecht, Holland, 1986.

[6] Thomas J. R. Hughes. Recent progress in the development and understanding of SUPG methods with special reference to the compressible Euler and Navier–Stokes equations. *Computer Methods in Applied Mechanics and Engineering*, 7:1261–1275, 1987.

[7] Thomas J. R. Hughes, Michel Mallet, and Akira Mizukami. A new finite element formulation for computational fluid dynamics: II. Beyond SUPG. *Computer Methods in Applied Mechanics and Engineering*, 54:341–355, 1985.

[8] Claes Johnson. *Numerical Solution of Partial Differential Equations by the Finite Element Method*. Cambridge University Press, 1987.

[9] D. D. Joseph and Y. Y. Renardy. Fundamentals of two–fluid dynamics, part II: Lubricated transport, drops and miscible liquids. *Springer, New York*, 1993.

[10] Christopher G. Koutitas. *Mathematical Models in Coastal Engineering*. Applied Mathematical Sciences. Pentech Press.

[11] N. P. Kruyt, C. Cuvelier, A. Segal, and J. Van Der Zanden. A total linearisation method for solving viscous free boundary flow problems by the finite element method. *International Journal for Numerical Methods in Fluids*, 8:351–363, 1988.

[12] L. D. Landau and E. M. Lifshitz. *Fluid Mechanics*. Pergamon, Oxford, 1987.

[13] J. Tinsley Oden, Noboru Kikuchi, and Young Joon Song. Penalty–finite element methods for the analysis of Stokesian flows. *Computer Methods in Applied Mechanics and Engineering*, 31:297–329, 1982.

[14] Bernard J. Omodei. Computer solutions of a plane Newtonian jet with surface tension. *Computers and Fluids*, 7:79–96, 1979.

[15] J. C. Simo and F. Armero. Unconditional stability and long–term behaviour of transient algorithms for the incompressible Navier–Stokes and Euler equations. *Computer Methods in Applied Mechanics and Engineering*, 111:111–154, 1993.

[16] N. M. J. Woodhouse. *Introduction to Analytical Dynamics*. Oxford Science Publications, 1987.